

# Changes in charge density vs changes in formal oxidation states: The case of Sn halide perovskites and their ordered vacancy analogues

Gustavo M. Dalpian,<sup>1,2,\*</sup> Qihang Liu,<sup>1,\*</sup> Constantinos C. Stoumpos,<sup>3,\*</sup> Alexios P. Douvalis,<sup>4</sup> Mahalingam Balasubramanian,<sup>5</sup> Mercouri G. Kanatzidis,<sup>3,6</sup> Alex Zunger<sup>1</sup>

<sup>1</sup>Renewable and Sustainable Energy Institute, University of Colorado, Boulder, Colorado 80309, USA

<sup>2</sup>Centro de Ciências Naturais e Humanas, Universidade Federal do ABC, Santo André, SP, Brazil

<sup>3</sup>Materials Science Division, Argonne National Laboratory, Argonne, Illinois 60439, USA

<sup>4</sup>Physics Department, University of Ioannina, 45110 Ioannina, Greece

<sup>5</sup>Advanced Photon Source, Argonne National Laboratory, Argonne, IL 60439, United States

<sup>6</sup>Department of Chemistry, Northwestern University, Evanston, Illinois 60208, USA

## Abstract

Shifting the Fermi energy in solids by doping, defect formation or gating generally results in changes in the charge density distribution, which reflect the ability of the bonding pattern in solids to adjust to such external perturbations. In the ionic limit, such changes are described by the formal oxidation states (FOS) whereby a single atom type is presumed to absorb the full burden of the perturbation (change in charge) of the whole compound. In this picture,  $\text{Co}^{3+}$  transforms to  $\text{Co}^{4+}$  when  $\text{LiCoO}_2$  is de-lithiated forming  $[\text{CoO}_2]$ ;  $\text{Cu}^{2+}$  transforms to  $\text{Cu}^{3+}$  when  $\text{La}_{2-x}\text{Ba}_x\text{CuO}_4$  is doped p type; and when the solar absorber  $\text{CsSnI}_3$  loses 50 % of its Sn atoms thereby forming the ordered vacancy compound  $\text{Cs}_2\text{SnI}_6$ , the Sn is said to change from  $\text{Sn}^{2+}$  to  $\text{Sn}^{4+}$ . In reality, the charge redistribution is more complex. Indeed, the particular patterns of charge rearrangements in response to shifts in the Fermi energy can inform us about the properties of the solid at hand:  $\text{CsSnI}_3$  (termed 113) with its Sn (II) FOS and  $\text{Cs}_2\text{SnI}_6$  (termed 216) with its Sn(IV) FOS can be viewed as ionic compounds denoted  $\text{Cs}^+(\text{SnI}_3)^-$  (analogous formally to  $\text{Cs}^+\text{I}^-$ ), yet they have relatively small semiconducting band gaps of the order of 1.3 eV, rendering them successful photovoltaic absorbers. On the other hand, the analogous  $\text{CsSrI}_3$  or  $\text{CsSrI}_3$  family of halides has much wider gaps, ( $\sim 4$  eV) and are thus useless as solar absorbers. To understand the electronic properties of these two groups and to gauge the trends in *s*-electron charge on the nucleus, we studied the 113/216 compound pairs  $\text{CsSnCl}_3/\text{Cs}_2\text{SnCl}_6$ ;  $\text{CsSnBr}_3/\text{Cs}_2\text{SnBr}_6$ , and  $\text{CsSnI}_3/\text{Cs}_2\text{SnI}_6$ . We have calculated the electronic structure of these three compound pairs, complementing them by  $\text{CsSnF}_3/\text{Cs}_2\text{SnF}_6$  in the hypothetical cubic structure for completing the chemical trends. These materials were also synthesized by chemical routes and characterized by X-ray diffraction,  $^{119}\text{Sn}$ -Mössbauer spectroscopy and K-edge X-ray Absorption Spectroscopy. We find that indeed in going from 113 to 216 (equivalent to the introduction of two holes per unit cell) there is a decrease in the *s* charge on Sn, in agreement with the FOS picture. However, at the same time, we observe an *increase* of the *p* charge via downshift of the otherwise unoccupied *p* level, an effect that tends to replenish much of the lost *s* charge. At the end, the change in the charge on the Sn site as a result of adding to holes to the unit cell is rather small. This effect is theoretically explained as a ‘self-regulating response’ [H. Raebiger, S. Lany, and A. Zunger, *Nature* **453**, 763 (2008)] whereby the system re-hybridizes to minimize the effect of the charge perturbation created by vacancy formation. Rather than having a single pre-selected atom (here, Sn) absorb the full brunt of the perturbation producing two holes/cell, we find that the holes are distributed in a complex pattern throughout the octahedral systems of  $\text{X}_6$  ligands, forming hole orbitals with some specific symmetries. Our work clarifies the relation between FOS and charge transfer that can be applied to a wide variety of materials.

## I. Introduction

The halide perovskites<sup>1</sup>  $A^I M^{IVB} X^{VII}_3$  (with A = organic or inorganic monovalent cation;  $M^{IVB}$  = metalloid Sn, Pb; and  $X^{VII}$  = Cl, Br, I) are successful as semiconducting *solar absorbers* (band gaps as low as 1.2 eV for  $CH_3NH_3SnI_3$  and 1.5 eV for  $HC(NH_2)_2PbI_3$ ). This is surprising, given that these compounds represent in essence *ionic halides*  $A^+[(Pb/Sn)X_3]^-$ . Indeed, analogous ionic compounds  $A^+[Ba/SrI_3]^-$  have far larger band gaps ( $\sim 4$  eV for  $CsSrI_3$ ), being insulators and useless as photovoltaic (PV) absorbers. We will see that we owe this special feature of PV-useful *small gap, formally ionic*  $A^I M^{IVB} X^{VII}_3$  compounds that have recently climbed to the top of the thin-film PV charts to the existence of bonding-viable latent *p* orbitals in the Sn but not in alkaline earth elements such as Sr/Ba.

The  $A^+[(Sn)X_3]^-$  (called 113) compounds need to be stabilized against loss of Sn, an oxidizing process that results ultimately in the ‘ordered vacancy compound’  $Cs_2Sn\Box X_6$  (called “216” compound, with 50% Sn vacancies<sup>2,3</sup>). The “proximity effect” of the unoccupied *p* orbitals to the bonding arena in  $CsSnX_3$  -- which allows such compounds to have low, PV-useful band gaps -- raises another interesting question regarding the role of the Sn valence electrons as one transforms  $CsSnX_3$  to  $Cs_2Sn\Box X_6$ : will Sn (IV) in the 216 compound (formally with configuration  $s^0 p^0$ ) also have effective *s-p* valence electrons as in Sn (II) (formally  $s^2 p^0$ ) in the 113 compound, but unlike Sr/Ba(II) (formally  $s^0$ )? This question is interesting because as is generally known,<sup>4</sup> formal oxidation states (FOS) such as Sn(II) and Sn(IV) do not imply complete removal of II or IV valence electrons, respectively, yet whatever residual physical valence charge density resides on Sn can control its electronic properties, including its solar band gaps. The broader question here is the general relationship between FOS and the physical valence charge density residing on bonded atoms when the compound as a whole loses charge. This general subject was debated as of late in the context of the so-called ‘self-regulating response’<sup>4</sup> and recently recalled in the context of Sn(II)/Sn(IV) in halide perovskites by Xiao et al.<sup>5</sup>

To address these questions, we synthesized and characterized (details of solution synthesis methods given in the Supplemental material section S1) several sets of  $CsSnX_3$  and  $Cs_2SnX_6$  compounds ( $X = Cl, Br, I$ ), as well as the reference binary compounds  $SnI_2$  and  $SnI_4$ . These materials were characterized by X-ray diffraction (see Supplemental Material S2) at the Advanced Photon Source at Argonne National Laboratory. We also performed  $^{119}Sn$ -Mössbauer spectroscopy and K-edge X-ray Absorption Spectroscopy (XAS) (details of characterization

techniques on Supplemental Material S2) to gauge the trends in s-electron charge on the nucleus. We have also calculated the electronic structure of these 113/216 compound pairs, complementing them by CsSnF<sub>3</sub>/Cs<sub>2</sub>SnF<sub>6</sub> in the hypothetical cubic structure for completing the chemical trends in that structure. Our calculations were performed by using the Density Functional Theory (DFT) within the Generalized Gradient Approximation for exchange correlation as implemented in the VASP<sup>6</sup> code. Details of the calculation method are reported in the Supplementary material S3. We use the experimental lattice structure determined by X-Ray refinement, allowing (as noted in the text) local relaxation of the atoms to zero force conditions. Band gaps and band structures were then calculated by using hybrid functional (HSE).<sup>7</sup>

From this extensive set of data, we find that:

(i) The existence of a multi-channel coupling (e.g., occupied s and empty p in the Sn compounds) enables a self-regulation response (SRR) whereby the system can minimize the effect of the external perturbation (removing 50% Sn from CsSnX<sub>3</sub>) by creating opposite and nearly compensating charge rearrangements between the different channels: reduction of s charge and enhancement of p charge on Sn. As a result, whereas the *formal* oxidation state of Sn is said to change from II in CsSnI<sub>3</sub> to IV in Cs<sub>2</sub>SnI<sub>6</sub>, the *physical charge densities* residing on the Sn atom computed by density functional theory (DFT) does not show significant changes. While the relative constancy of physical charge density around bonded atoms subjected to Fermi level altering events can be suspected on general bonding heuristics, the nonlinear mechanism causing this charge resilience is not trivial. The multi-channel s-p mechanism resembles a Le Chatellier-like response, minimizing perturbations.

(ii) The change in s electrons is clearly captured by the Mössbauer isomer shift, in good agreement with DFT calculations of this quantity.

(iii) Calculated differences in 113 and 216 charge densities at constant geometries identify locations in the unit cell where the two holes produced by removal of 50 % of Sn are actually distributed. Rather than having a single pre-selected atom absorb the full brunt of the perturbation producing two holes/cell, as classically envisioned by the FOS concept, we find that the holes are distributed in a complex pattern throughout the octahedral systems of X<sub>6</sub> ligands, forming hole orbitals with some specific symmetry.

(iv) The above noted SRR is active when the cation sublattice is strongly coupled to the anion sublattice, enabling compensating exchange of s and p carriers. The classic ionic limit where

such communication is disabled exists to some extent in the hypothetical cubic  $\text{ASnF}_3/\text{A}_2\text{SnF}_6$  fluoride where loss of s electrons is not compensated by gain of p electrons. A more nearly ideal weak-coupling (ionic) limit is revealed in  $\text{CsSrI}_3$  lacking active valence p electrons. DFT calculations show that the charge resides solely in the s channel, resulting in far wider band gaps than in the covalent systems capable of SRR, and thus enabling solar absorption in the latter but not the former.

Our work provides microscopic, quantum-mechanical content and predictive details of the relation between FOS and actual charge transfer. The concept described here not only provides an alternative thinking of the fundamental physical chemistry process of response to charging in strongly- coupled orbital systems, but also sheds light on a wide variety of systems with significant ion-ligand hybridization, in addition to halide perovskites, such as materials with multivalence and with strong correlation effect.

## II. The broader issue of FOS, charge density and Self-Regulating Response

One generally needs to discuss *changes* in charges that result from a redox perturbation, not absolute charges. Indeed, it was established in condensed matter physics that while static atomic charges in a solid are ill defined, the *charges displaced by any perturbation* ('charge in transit') are unambiguous.<sup>8,9</sup> At the root of this are the *continuity equation*, and the fact that currents (either steady state or transient) are well defined in condensed-matter theory.

The concept of FOS of an ion is connected with the idea of charge transfer<sup>10</sup>. It is commonly defined as

$$\text{FOS}(\text{ion}) = Q(\text{compound}) - \sum Q(\text{ligands}) \quad (1)$$

Here, the first term on the right-hand side is the observable *physical* charge of the system as a whole. For molecules, it equals the net ionic charge, e.g., +1 for  $[\text{NH}_4]^+$  or -1 for  $[\text{BH}_4]^-$ ; for solids such charges are commonly induced by shifting the Fermi level via carrier doping. The second term corresponds to the sum of the presumed phenomenological effective charges on ligands. Its magnitude could be guessed from the relative electronegativities of the ligand vs. central ion. For example, it is +4 for the hydrogen  $\text{H}_4$  ligand in  $[\text{NH}_4]^+$  and -4 for the hydrogen  $\text{H}_4$  ligand in  $[\text{BH}_4]$ . Eq. (1) incorporates, as the first term a physical (observable) net charge, but the second term is a non-observable set of charges whose magnitude, as will be illustrated, lies to a large extent in the eyes of the beholder. Indeed, the determination of  $Q(\text{ligand})$  might require

sometimes a deeper understanding of the ligand-to-ion bonding than supplied by the respective electronegativities. As a result of this model-dependence of the second term in Eq. (1) the concept FOS(ion) is sometimes problematic as a useful tool. Whether the FOS represent a physical charge residing on a specific atom has a long-term debate starting from Pauling in 1948,<sup>11</sup> and then supported by R. Hoffmann in 2001,<sup>12</sup> claiming that the charge of +6 on iron in  $[\text{FeO}_4]^{2-}$  and  $-2$  in  $[\text{Fe}(\text{CO})_4]^{2-}$ , as suggested by FOS, is impossible. As shown by Sawatzky and coworkers<sup>13</sup> for the perovskite rare-earth nickelates ( $\text{RNiO}_3$ ), Ni behaves like 2+ (rather than 3+) in a normal high-spin state ( $S = 1$ ), and there is one hole per 3 oxygens in the O  $2p$  band of states.

Despite this, the FOS axiom is a numerical estimate of the electronic state of matter that has helped in the development of chemistry using simple, intuitive concepts. Using FOS, a chemist can interpret the preferred geometry of a molecule, or why a chemical bond is shorter than another for a set of compounds with different oxidation numbers. In the specific case of Sn halide compounds examined here ( $\text{CsSn}^{\text{II}}\text{X}_3/\text{Cs}_2\text{Sn}^{\text{IV}}\text{X}_6$ ), as the formal oxidation state increases, the Sn-X bond length decreases. This can be said to be due to an increase in the electronegativity of Sn as its FOS increases. At the same time, measured bond lengths tell us that assuming ideal (integer values) of FOS as in  $\text{CsSn}^{\text{II}}\text{X}_3$  and  $\text{Cs}_2\text{Sn}^{\text{IV}}\text{X}_6$ , does not fully capture such FOS trends, and adding a secondary coordinates of ionicity/covalence to FOS is needed to rationalize the trends. This is suggested by the fact that the bond lengths of the  $\text{CsSn}^{\text{II}}\text{I}_3$  extended solid (perovskite) and the  $\text{Cs}_2\text{Sn}^{\text{IV}}\text{I}_6$  molecular salt ( $\text{K}_2\text{PtCl}_6$ -type) lie *in between* the two cases of  $\text{Sn}^{\text{IV}}\text{I}_4$  and  $\text{Sn}^{\text{II}}\text{I}_2$  which consist of covalent in the former case and (primarily) ionic Sn-I bonds in the latter case, respectively (Figure S1). (That  $\text{SnI}_4$  is more covalent is signaled by its tetrahedral geometry in contrast with the more ionic compounds  $\text{Cs}_2\text{Sn}^{\text{IV}}\text{X}_6$ ,  $\text{CsSn}^{\text{II}}\text{X}_3$  and  $\text{SnI}_2$  which adopt an octahedral coordination). The need to refine the classic FOS concept by adding the independent coordinates of covalency/ionicity will feature prominently in our understanding of the degree to which FOS reflects the physical charge density distribution in compounds.

The discussion above can be posed as a quantum mechanical computational problem: According to Eq. (1), a change of the electron count [i.e., a change of  $Q(\text{compound})$ ] necessitates that the FOS (ion) of one ion must change. Will the *physical charge density* around the ion change too? It was theoretically reported early on that, for  $3d$  impurities in silicon and GaAs,<sup>14</sup> and for the de-lithiation process of  $\text{LiCoO}_2$ ,<sup>15</sup> the physical charge density stayed nearly constant as  $Q(\text{compound})$  was varied. This is the essence of the self-regulating response (SRR): in a

system where metal ions and ligand form coupled quantum states, when the system is perturbed by reducing the compounds charge (shifting the Fermi energy), the ligands re-hybridize self-consistently (including the possibility of atomic displacements), thereby replenishing much of the charge lost by the cation; the physical charge on the cation is therefore largely unchanged, even though the FOS would change by integer numbers. Here we examine the way the physical charge density changes in the  $\text{ASnX}_3$  compounds when two holes are introduced into the unit cell by creation of extensive Sn vacancies, comparing the result to the FOS rendering of the same event. The availability of X-ray diffraction, as well as  $^{119}\text{Sn}$ -Mössbauer spectroscopy and K-edge XAS provides crucial evidence, supporting the results of the theory.

### III. Considering s electrons on Sn: experimental and theoretical probes

#### A. The Mössbauer spectroscopy and its DFT interpretation

If the charge on Sn(II) /Sn(IV) were purely due to absence or presence of s-electrons (as in the extreme ionic picture), what would the chemical trends in perturbed charge densities be? To address this question,  $^{119}\text{Sn}$  Mössbauer spectroscopy is used to probe directly the electron population residing in the s-orbitals (see Supplementary Materials S2 for experimental details). This is expressed by the difference in the isomer shift (IS) between a reference material (here  $\text{SnO}_2$ ) and the perovskite sample. This is exemplified by the Mössbauer spectra of  $\text{CsSn}^{\text{II}}\text{Br}_3$  and  $\text{Cs}_2\text{Sn}^{\text{IV}}\text{Br}_6$ , with both compounds having a similar coordination, adopting a cubic symmetry at room temperature (see Figure 1a). The experimental spectra of  $\text{Cs}_2\text{SnBr}_6$ , with a FOS of IV, resonates at  $\text{IS} = 0.83 \text{ mm/s}$  while  $\text{CsSnBr}_3$ , with a FOS of II, has a resonance at  $\text{IS} = 3.90 \text{ mm/s}$ . These values clearly indicate that the relative s-orbital charge distributions of  $\text{SnO}_2$  is much closer to  $\text{Cs}_2\text{SnBr}_6$  than to  $\text{CsSnBr}_3$ , thus fully supporting the FOS picture. Similar trends occur in other compounds of the  $\text{CsSnX}_3$  and  $\text{Cs}_2\text{SnX}_6$  families and the experimental results are listed in Table S1. The results are in excellent agreement with previously reported values.<sup>16,17,18</sup> Note that we chose not to include experimental data for  $\text{CsSnCl}_3$ <sup>19</sup> and  $\text{CsSnI}_3$ <sup>20</sup> in this table since these compounds have non-perovskite polymorphs (different coordination environments) which may introduce discrepancies in the experimental trends. The Mössbauer spectra of these compounds have been reported previously by Donaldson et al.<sup>21</sup>

Theoretically, the isomer shift arises from the *difference* of electronic wavefunction density at the nuclear site ( $\Delta\rho_{Sn}(0)$ ) of both the target absorber and source. Giving a specific source reference (in this work we use SnO<sub>2</sub>), the isomer shift of Sn ( $\delta$ ) is expressed as<sup>22</sup>

$$\delta = \frac{2\pi Zce^2}{3E_\gamma} \Delta\rho_{Sn}(0) \cdot \Delta\langle r^2 \rangle, \quad (2)$$

where  $Z = 50$  is the atomic number of Sn, and  $c$ ,  $e$ ,  $E_\gamma$  and  $\Delta\langle r^2 \rangle$  denote the speed of light, electron charge, the  $\gamma$ -ray energy and the mean square nuclear radius for the transition, respectively. The coefficient  $\Delta\rho_{Sn}(0) = \sum_{occ} (|\psi_A(0)|^2 - |\psi_S(0)|^2)$  counts the electron density (the sum of all occupied wavefunction square) at the nuclear site with  $r = 0$ .

Figure 1 shows the correlation between the experimentally measured isomer shift (Fig. 1a) and the DFT-calculated (see details in Appendix Methods) electron density difference at the nucleus  $\Delta\rho_{Sn}(0)$  on series of Sn based halide compounds. We find an excellent linear correlation between the two quantities, indicating that DFT is a good predictor of IS. Similarly, good correlation was reported for other Sn-based compounds when referenced to SnO<sub>2</sub>.<sup>22</sup>

Although  $\Delta\rho_{Sn}(0)$  is the accurate quantity to correlate with the IS, a more intuitive (but less rigorous) quantity is the charge *around* a bonded atom, as it has an intrinsic scale (such as  $< 2$  for  $s$ -electrons). The total and angular-momentum ( $l$ ) decomposed atomic charges are defined and calculated by projecting the periodic wave functions  $\psi_n(\mathbf{k})$  (expressed with plane-wave expansion) on spherical harmonics of Sn site  $i$  and summing over all occupied bands:

$$Q_{i,l} = \sum_{n,k}^{occ} \langle \psi_n(\mathbf{k}) | (|l, i = Sn\rangle \langle l, i = Sn|) | \psi_n(\mathbf{k}) \rangle, \quad (3)$$

where  $|l, i\rangle$  is the angular momentum eigenstate of  $i$ -th atomic site. Here we consider only Sn 5s atomic charge ( $l = 0$ ).

Figure 1c shows that the measured  $Q_{Sn5s}$ . IS correlates well with the s-like atomic charge around the bonded Sn atom. As expected, the 113 compounds have more s-charge [ $Q(\text{Sn}) \sim 2$ ] than the 216 compounds [ $0.5 < Q(\text{Sn}) < 1$ ]. Interestingly, one can delineate two separated groups in Fig. 1c, indicated by ellipses: the compounds that are normally associated with a formal oxidation state of 4+ (SnX<sub>4</sub>, Cs<sub>2</sub>SnX<sub>6</sub>) have less s charge than those associated normally with a 2+ FOS (SnX<sub>2</sub>, CsSnX<sub>3</sub> and CaSnO<sub>3</sub>). If there were no p electrons as suggested by the ionic picture [Sn(II):  $s^2p^0$  and Sn(IV):  $s^0p^0$ ], and no charge density outside atoms ('extra-atomic charge') *this result will imply an association of 113 compounds with FOS=II and 216 compounds with FOS=IV.*

## B. X-ray Absorption Near Edge Structure as a direct probe of the effective charge on Sn relative to its metallic state ( $\text{Sn}^0$ ).

The generally accepted methods of determining the oxidation state of metals include Photoemission Spectroscopy (PES), X-ray Absorption Near Edge Structure (XANES). PES, and in particular X-ray Photoemission Spectroscopy (XPS), is a widely used method which probes the M electron shell ( $3d$  orbitals) in 1-1000eV spectral range and it is invaluable for assessing the FOS of transition metals. In the case of Sn, however, this method has been shown to be quite insensitive, as in this case, as illustrated here, FOS does not take up the ideal value of the s orbital occupation (FOS=II being  $s^2$  and FOS=IV being  $s^0$ ); instead, here FOS reflects a range of electron population of the 5s states.<sup>23,24</sup> In other words, the ideal integer FOS do not by themselves reflect the electron distribution in different Sn(II) and Sn(IV) compounds, and an additional, independent factor exists—the actual s electron count. Ultraviolet Photoemission Spectroscopy (UPS), which probes the electrons on top of the valence band (0-20eV) and in principle can provide answers with respect to the FOS of Sn, is very sensitive to the surface of the sample and is prone to vary when measured on different thin-film substrates.<sup>25</sup> In order to ensure that the observed trends arise from the bulk materials alone, all samples were characterized by powder X-ray diffraction (PXRD) to eliminate the possibility of secondary phases (Figures S2-S6).

The obtained XANES spectra (Figure 2) are characterized by the Sn absorption edge corresponds to the ionization of one 1s electron, which occurs at  $E_i = 29200.4$  eV for the Sn metal,<sup>26</sup> and an above edge peak which corresponds to the transition probability of the 1s electron to the empty 5p orbitals ( $\Delta l = \pm 1$  selection rule) to form a core-hole/photo-electron pair (exciton). As the FOS of Sn increases so does the ionization energy and as a result the K-edge absorption shifts to higher energies. It is clearly seen from Figure 2 that compounds with a II FOS ( $\text{SnI}_2$ ,  $\text{CsSnBr}_3$ ) have a similar absorption energy, whereas the IV FOS compounds ( $\text{SnI}_4$ ,  $\text{Cs}_2\text{SnX}_6$ ) have a significantly higher absorption edge energy. However, we can not tell if the increase of the ionization energy reflects a large ( $\sim 2e$ ) or small reduction of s orbital count .

Interestingly, the absorption edge energy in the IV FOS compounds increases proportionally with the electronegativity of the halide ( $\chi_{\text{Cl}} > \chi_{\text{Br}} > \chi_{\text{I}}$ ) whereas in the II FOS compounds (Figure 2) the absorption edge is insensitive to the electronegativity of the halide. This trend parallels the

DFT results in Fig. 1c and implies that when the  $5s^2$  lone pair is present the ligands do not affect the  $s$  charge whereas its absence in the  $\text{Sn}^{4+}$  ions allows the electronegativity of the ligand be the charge-determining factor. This observation is also in good agreement with both Mössbauer spectroscopy and DFT calculations, providing an independent confirmation of the electron populations on Sn orbitals.

The IS values of the  $\text{Sn}^{4+}$  ions with  $\text{I}^-$ ,  $\text{Br}^-$  and  $\text{Cl}^-$  environments in the  $\text{Cs}_2\text{SnX}_6$  series also follow a trend (similar as that found for the "model"  $\text{SnX}_4$  compounds,<sup>27</sup> where the decrease in IS values is related to the decrease in  $5s$  electron density at the  $^{119}\text{Sn}$  nucleus, due to the decreasing covalency of the Sn-X bond as the  $p$ -orbital configuration changes from  $5p$  (I) to  $4p$  (Br) to  $3p$  (Cl).<sup>28</sup> On the other hand, the spectra of II FOS compounds ( $\text{SnI}_2$ ,  $\text{CsSnBr}_3$ ), which consistently show an IS = 3.90 mm/s irrespective of the halide or the coordination environment. As shown in Figs. 1b and 1c, the FOS II group the different compounds are clustered, while for the FOS IV group they are more sparsely distributed. Compared with FOS II group that has almost all  $s$  electrons occupied, FOS IV group has part of the  $s$  electrons ionized.

A second trend that appears from the XANES spectra comes from the intensity of the exciton peak as a function of the halide ligand. The intensity of the exciton peak relates directly to the probability of the  $5p$  orbitals to be occupied by the excited photo-electron and it serves as an indirect measure of the occupation of the Sn orbitals in the Sn-X bonding. This quantity directly relates with the electronegativity difference between Sn and X; the higher the difference the more ionic the bond and the more orbitals are accessible to the photo-electron during the  $1s$ - $5p$  transition. This trend is confirmed in Fig. 2, where all the compounds displaying a comparable peak intensity for the same halide ligands.

#### IV. The $p$ charge on Sn in strong-coupling Iodide systems

To understand the extent to which the ionic limit is obeyed by these Sn-based compounds, we show in Figs. 3a and 3b the DFT-calculated density of states (DOS) of  $\text{CsSnI}_3$  and  $\text{Cs}_2\text{SnI}_6$ , respectively, and the electronic charge density (Fig. 2c) describing some of the DOS peaks that are important to our analysis. This associates the "s charge"  $Q_{\text{Sn}5s}$ , discussed in the previous section with certain energy windows in the DOS, thus providing better insights into the origin of this charge. Not surprisingly, the electronic charge density enclosed in the DOS energy window corresponding to Peak I (in  $\text{CsSnI}_3$ ) and II (in  $\text{Cs}_2\text{SnI}_6$ ) clearly shows ***5s charge*** in both

compounds (Fig. 3c). The 216 compound has less 5s charge around the Sn atom, as evidenced also from the Mössbauer data (Fig 1). However, analysis of the Sn **5p charge** for both compounds reveals important differences: comparing the charge density plots (Fig. 3c) of peak I (CsSnI<sub>3</sub>) to II (Cs<sub>2</sub>SnI<sub>6</sub>) we see *a decrease of 5s charge density around Sn*, but comparing the charge density plots of peaks III (CsSnI<sub>3</sub>) to IV (Cs<sub>2</sub>SnI<sub>6</sub>) we see *an increase of 5p charge density around the Sn atom*. Thus, Sn tends to preserve its total charge in the face of a perturbation that reduces its s-charge by removing 50% of the Sn atoms.

Moving from charge *density* maps (Fig. 3c) to angular dependent atomic charge Eq. (3), and considering the difference in total charge on Sn between CsSnI<sub>3</sub> and Cs<sub>2</sub>SnI<sub>6</sub>, we find the difference is surprisingly small. Our calculations show that while the Sn atom in CsSnI<sub>3</sub> loses 0.6 s electrons when it is transformed to Cs<sub>2</sub>SnI<sub>6</sub>, it gains back 0.2 p electrons in the occupied state, so the change in total physical charge on the Sn atom is just 0.4 e. While the s charge is reduced upon removal of Sn atoms from the (113) compound (oxidation), non-s charge acts to offset the decrease in s charge so the physical charge on Sn is similar in 113 and 216. Specifically, while in the ionic limit the valence states of Sn are written as Sn(II): s<sup>2</sup>p<sup>0</sup> and Sn(IV): s<sup>0</sup>p<sup>0</sup>, in the covalent case the valence states are written as Sn(II): s<sup>2</sup>p<sup>m</sup> and Sn(IV): s<sup>2-Δ1</sup>p<sup>m+Δ2</sup>. Accordingly, the charge difference on Sn is Δ1-Δ2, rather than +2 suggested by FOS in the ionic limit. This is a manifestation of the self-regulation response: keeping the physical charge nearly constant and delocalizing the holes in the X ligands. Thus, one does not expect to find a good correlation between the isomer shift and the **total** physical charge on Sn (see Fig. S1 in the supplementary section), indicating that the total charge on Sn cannot reflect FOS in covalent compounds. *Such a SSR effect is very general and is seen in other systems as well.*

Previous study focusing on the oxidation state of Sn in Cs<sub>2</sub>SnI<sub>6</sub> concluded that the oxidation state of Sn in this material should be the (II), the same as in CsSnI<sub>3</sub>.<sup>5</sup> This would occur because the Sn 5s orbitals would be occupied in both compounds. Our calculations show that this is not the case: The Sn 5s orbitals in 216 are half occupied, while in 113 Sn 5s is completely occupied. Also, previous work disregarded the effect of Sn 5p orbitals. The Sn 5p state in 216 has SSR effect, compensating the loss of 5s charge compared with 113 compound. The facts presented here and not considered before are important to get a complete understanding of charge self-regulation in these compounds.

## V. Energy level model that explains the $s$ vs $p$ negative feedback in the strong coupling limit of the $\text{CsSnI}_3$ and $\text{Cs}_2\text{SnI}_6$ compounds

Going back to the specific case of 113 vs. 216 Sn compounds, we develop an energy level diagram distilled from our DFT calculations that explains the mechanism of the negative feedback (Fig. 3d). The hybridization between the Sn( $5s$ ,  $5p$ ) at the center and the octahedron of I $5p$  ions is governed by symmetry considerations. Specifically, while the Sn atom has spherical  $s$  states and dumbbell  $p$  states, the I $_6$  cage has  $O_h$  point group and their  $p$  orbitals are split to several representations. Among them, only the states with  $A_{1g}$  symmetry (singlet, basis function  $x^2+y^2+z^2$ ) can hybridize with Sn  $5s$  states, while I $5p$   $T_{1u}$  states (triplets, basis function  $x$ ,  $y$ ,  $z$ ) couple with Sn  $5p$  states. The remaining representations of I $_6$  ( $e_g$ ,  $T_{1g}$ ,  $T_{2g}$ ,  $T_{2u}$ , etc.) simply have no counterpart in Sn to bond to, and are non-bonding. In Fig. 3(a) and (b), the projected DOS of the hybridization between Sn $5s$  and I $5p$   $A_{1g}$  orbitals, and between Sn $5p$  and I $5p$   $T_{1u}$  orbitals are shown by red and green highlights, respectively. For each pair of hybridized states, the lower energy part indicates bonding state, and the higher energy part indicates the antibonding state.

Using the calculated DOS we are able to explain the SRR effect by simplifying the projected DOS into a 4-level model (corresponding to the 4 peaks in Fig. 3a and b). As shown in the schematic plot in Fig. 3d, from 113 to 216 the Sn-I coupling becomes stronger because of the 8% shrink in the size of SnI $_6$  octahedra (supplementary S3). For the Sn $5s$  and I $5p$ - $A_{1g}$  pair, in 113 both the bonding and antibonding states are occupied, so the Sn  $5s$  orbitals are fully occupied. In contrast, the stronger hybridization pushes the antibonding state above the Fermi level, leading to a loss of occupied Sn  $5s$  electron. At the same time, hybridization also depopulates some I $5p$  states, which distribute equally in the I $_6$  octahedra, forming  $A_{1g}$  hole orbitals. *On the other hand, the Sn  $5p$  orbital, while often neglected, accepted electron density from the Iodine ligands and plays a crucial role on compensating the total charge of Sn. The bonding state of Sn  $5p$  and I $5p$ - $T_{1u}$  is occupied for both 113 and 216 compounds, indicating that there is always electron density in the Sn  $5p$  orbitals.* Compared with 113, stronger hybridization in the 216 systems mixes even more Sn  $5p$  orbitals with the occupied bonding state which is predominantly I $5p$  based. Consequently, when the antibonding Sn  $5s$  electrons get depopulated in response to the formation of Sn vacancies, the Sn  $5p$  character of occupied orbitals is increased, compensating the loss of  $s$  electrons. Such a self-regulation response is a nontrivial, Le Chatelier-type response that happens in heavily covalent systems.

## VI. Charge density deformation maps for the strong coupling iodine compounds: where do the two holes go to?

The removal of 50% of the Sn atoms when one goes from the 113 to the 216 compounds is an oxidation and can be considered as a strong perturbation. Considering the results presented above, another question would be: where do the two holes produced by the 113 to 216 transformation reside if the physical charge on Sn does not change much?

Looking at the charge deformation map we can see the redistribution of charges. This is defined as  $\Delta\rho = \rho^{113} - \rho^{216} - \rho^{Sn}$ , where  $\rho^{113}$  and  $\rho^{216}$  refers to the total valence charge density of CsSnI<sub>3</sub> and Cs<sub>2</sub>SnI<sub>6</sub>, respectively.  $\rho^{Sn}$  is the charge density of the sublattice of Sn that is removed, and is used to balance the total charge difference. By necessity we use a *fixed geometry* for all the components either in the lattice parameter of the 113, in Fig. 4a, or the lattice parameter of the 216 compound, as show in Fig. S6. Both cases give similar results. The position of the Sn atoms, Sn vacancies and I atoms are indicated and a density profile along a representative line (Fig. 4b) gives a better idea of the amplitude of the differences. Blue areas indicate negative values.

When we go from the 113 to the 216 compounds there is a small but noticeable charge migration from the Sn atom to the Sn-I bond. The small change in the charge around the Sn atom corroborates that the charge sitting on the Sn atom is very similar for both compounds. Owing to the reconfiguration of charges away from the center of atoms, it is also clear that we move from a more ionic (113) to a more covalent (216) compound. *We see how the SRR works – charge is redistributed into positive (red) and negative (blue) oscillating domains so that the perturbation in physical charge upon vacancy formation is minimal.*

## VII. Moving along the series from strong-coupling covalent to the weak-coupling ionic limit (I→Br→Cl→F)

The discussion above on the SRR pertains to systems where there is strong coupling between the ligand subsystem and the metal subsystem as in the CsSnI<sub>3</sub>/Cs<sub>2</sub>SnI<sub>6</sub> cases. We consider next halide compounds with increasing electronegativity by using X = I, Br, Cl and F in CsSnX<sub>3</sub>/Cs<sub>2</sub>SnX<sub>6</sub>. The atomic charges  $Q_{i,l}$  of Eq. (3) for Sn 5s and 5p orbitals are shown in Figs. 5a and 5b respectively. We find that in the 113→216 perturbation, the Sn atom loses 0.60, 0.85,

1.04 and 1.31  $5s$  electrons for  $X = \text{I, Br, Cl}$  and  $\text{F}$ , respectively, indicating the increasing ionic component of the  $\text{Sn-X}$  bonds. In contrast, for  $X = \text{I}$  and  $\text{Br}$ ,  $\text{Sn } 5p$  atomic charges provide a compensation to the loss of the  $s$  electrons through an increase in the quantity of  $p$  electrons going from the 113 to the 216 compound, owing to the SSR effect we have described above. The SSR effect is diminishing as one increases the electronegativity of the  $X$  element. *For  $X = \text{F}$ , both  $\text{Sn } s$  and  $p$  components are losing charge, indicating that the two holes are mostly localized on the  $\text{Sn}$  atom, consistent with the FOS picture.* Clearly, in the extreme ionic limit of this series ( $X=\text{F}$ ), the SRR is almost gone. Indeed,  $\text{F}$  represents an electronic phase transition relative to  $X=\text{I, Br, Cl}$ : By looking at the energetic order of the atomic levels related to  $\text{Sn}$  and the halogen atoms, we find that *while for  $\text{I, Br}$  and  $\text{Cl}$  the halogen  $p$  orbital is above the  $\text{Sn}5s$  orbital (as in Fig. 3d), for the fluoride the  $2p$  orbital is below  $\text{Sn}5s$ .* This qualitative change is illustrated in Fig. S7, where we present the corresponding diagram. This reversed order of energy levels weakens the coupling between  $\text{Sn}5p$  and  $\text{F}2p$  levels, minimizing the SRR effect.

The maintenance of some  $\text{Sn } 5s$  charge even for the  $\text{F}$  compounds shows that even our most ionic compound cannot be considered fully ionic. It is instructive to look further for a perfect “no SRR” or ‘fully ionic’ case in this family. The best candidate is obtained by replacing  $\text{Sn}$  by a divalent cation with totally inactive (high energy)  $p$  states such as  $\text{Ba}$  or  $\text{Sr}$ . We have simulated  $\text{CsSrI}_3$  and observed the contribution of the  $\text{Sr}$  atom to the electronic structure. A projected density of states is shown in Supplementary material S6. *We observe that  $\text{Sr } 5s$  has a very small contribution to the occupied states, and the component of  $\text{Sr } 5p$  is negligible.* These are indications that the FOS of  $\text{Sr}$  in  $\text{CsSrI}_3$  agrees well with the classic FOS picture  $\text{Sr(II): } 5s^0 5p^0$ . Indeed, it is quite rare to find such almost ideal ionic FOS systems, as some metal-to-ligand coupling is ubiquitous.

### VIII. Band gaps of 113 vs 216 halide compounds

The absorption spectra of the halides show a consistent increase in the band gap as we move from  $\text{I}$  to  $\text{Br}$  and to  $\text{Cl}$ . The increase of the band gap is much larger for the 216 compounds than for the 113 compounds, as shown in the absorption spectra in Fig. 6a. While in  $\text{CsSnX}_3$  the band gap lie between  $E_g = 1.3 - 2.7$  eV ( $X = \text{I, Br, Cl}$ ), the band gaps of  $\text{Cs}_2\text{SnX}_6$  span across the much wider range  $E_g = 1.3 - 4.4$  eV ( $X = \text{I, Br, Cl}$ ), with  $\text{CsSnI}_3$  and  $\text{Cs}_2\text{SnI}_6$ , remarkably, starting from the same initial value. Fig. 6b shows the absorption spectra for  $\text{SnI}_4$  and  $\text{SnI}_2$ .

These trends can be better visualized in a schematic diagram: Figure 7a shows the measured bandgap trends for these compounds, whereas Fig. 7b shows the calculated bandgaps using a hybrid exchange-correlation functional (HSE). The calculated band gaps are smaller than experiment, as expected for this kind of calculations, although the chemical trends illustrated by the vertical arrows showing the differences in gaps, are similar.

The band structures are shown in Supplementary Fig. S6, reporting a direct band gap for all compounds. The band gap of the 113 compound is at R, whereas for the 216 compounds are at  $\Gamma$ . The dispersion in the 216 bands are very small, since  $\text{SnX}_6$  are isolated in these compounds.

The increase in the band gap for this 113/216 series of halides can be partially understood by considering the transition between 113 to 216 in distinct computational steps that isolate specific effects. There are three effects that are important to understand this effect: (i) the 216 compound is formed by removing Sn atoms from the 113 compound. The formation of these Sn *vacancies* is found to decrease the band gap, by the formation of *impurity-like* bands in the original gap. These *intermediate bands* can be clearly observed in the band structures in Fig. S7. (ii) The *intermediate bands* will change the character of the CBM in the 216 compounds. For 113 the VBM is composed of halide *p* levels, and CBM is mostly composed of Sn *p* levels. For the 216 compounds, the VBM is also composed of halide *p* levels, but the CBM comes from Sn *s* levels. (iii) The lattice parameter of the 216 compounds is smaller than the corresponding 113. This hydrostatic effect will increase the band gap. At the end, the competition between the creation of impurity levels (decrease the band gap) and hydrostatic effects (increase of the bandgap) explain the similar band gap for iodides and much larger bandgap for bromides and chlorides.

## IX. Summary and conclusions

SRR occurs in systems with significant ion-ligand hybridization, manifesting a strong covalent bonding between ion and ligands. The concept of SRR provides microscopic quantum-mechanical content and predictive details described throughout this paper, applicable to a broad range of metal-ligand feedback systems to what can be generally described phenomenologically in Freshmen Chemistry as *FOS-dependent electronegativity* [say, of Sn(II) becoming ‘less ionic and more covalent’ than Sn(IV)]. However, essential details defining the context of the SRR (such as the interplay between occupied and unoccupied orbitals responding oppositely to perturbations; and the way the holes are distributed in space) remain *ex-post-facto* descriptive

rather than *predictive*, indeed not just a difference in language.

This work discussed correlations between formal oxidation states of atoms and the actual charge density residing in that atom. We show, using Sn-based halide perovskites as prototype materials, that a self-regulating response is observed when these materials are subjected to strong perturbations. In our case the perturbation was the removal of 50% of the Sn atoms when we go from  $\text{CsSnI}_3$  to  $\text{Cs}_2\text{SnI}_6$ . The SSR acts in such a way that the charge density residing on the Sn atom in both cases is almost equal, although the formal oxidation state in both changes from Sn(II) to Sn(IV).

Our conclusions are supported by extensive *ab initio* calculations and experimental measurements including X-ray diffraction, Mossbauer spectroscopy and XANES, showing the nature of the compensating mechanism in these systems: while the Sn s charge decreases when going from  $\text{CsSnI}_3$  to  $\text{Cs}_2\text{SnI}_6$ , the Sn p charge actually increases. The idea of a self-regulating response should span to other systems, making our conclusions useful also for other types of materials.

### **Acknowledgements**

The work at the University of Colorado Boulder was supported by the U.S. Department of Energy, Office of Science, Basic Energy Sciences, Materials Sciences and Engineering Division under Grant No. DE-SC0010467 to C.U. Work at Northwestern University was supported by grant SC0012541 from the US Department of Energy, Office of Science. Use of the Advanced Photon Source at Argonne National Laboratory was supported by the Basic Energy Sciences program of the US DOE Office of Science under contract DE-SC0010467. GMD thanks financial support from Brazilian agencies FAPESP and CNPq. This work used resources of the National Energy Research Scientific Computing Center, which is supported by the Office of Science of the U.S. Department of Energy under Contract No. DE-AC02-05CH11231.

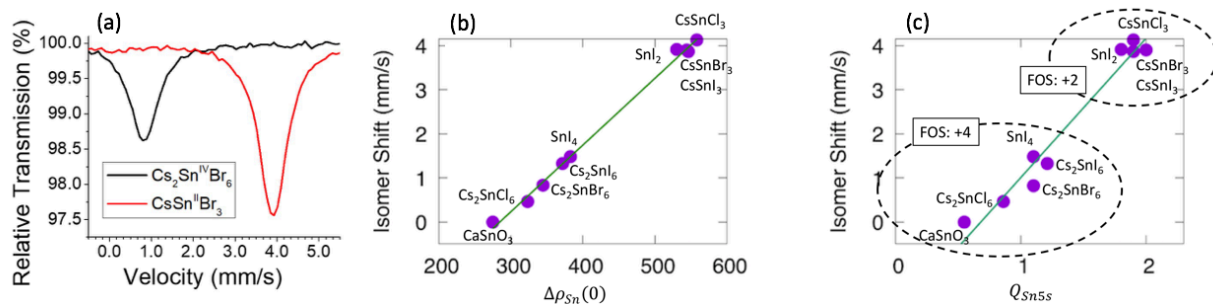


**Fig. 1:** (a) Room temperature  $^{119}\text{Sn}$  Mössbauer spectra spectra of  $\text{CsSnBr}_3$  and  $\text{Cs}_2\text{SnBr}_6$  relative to  $\text{SnO}_2$ . The relative transmission of the spectra is consistent with the concentration of Sn centers in  $\text{Cs}_2\text{SnBr}_6$  relative to  $\text{CsSnBr}_3$  (b) Correlation of experimental  $^{119}\text{Sn}$  isomer shifts (IS) of Mössbauer effect and the valence charge densities at Sn nuclear calculated by DFT. (c) The correlation between measured IS and the DFT calculated *occupied s charge around Sn*. The reference source is  $\text{CaSnO}_3$ , and the green line is the linear fit. The IS of  $\text{CsSnCl}_3$  and  $\text{CsSnI}_3$  are taken from Ref. 21, while the others are from our measurements.

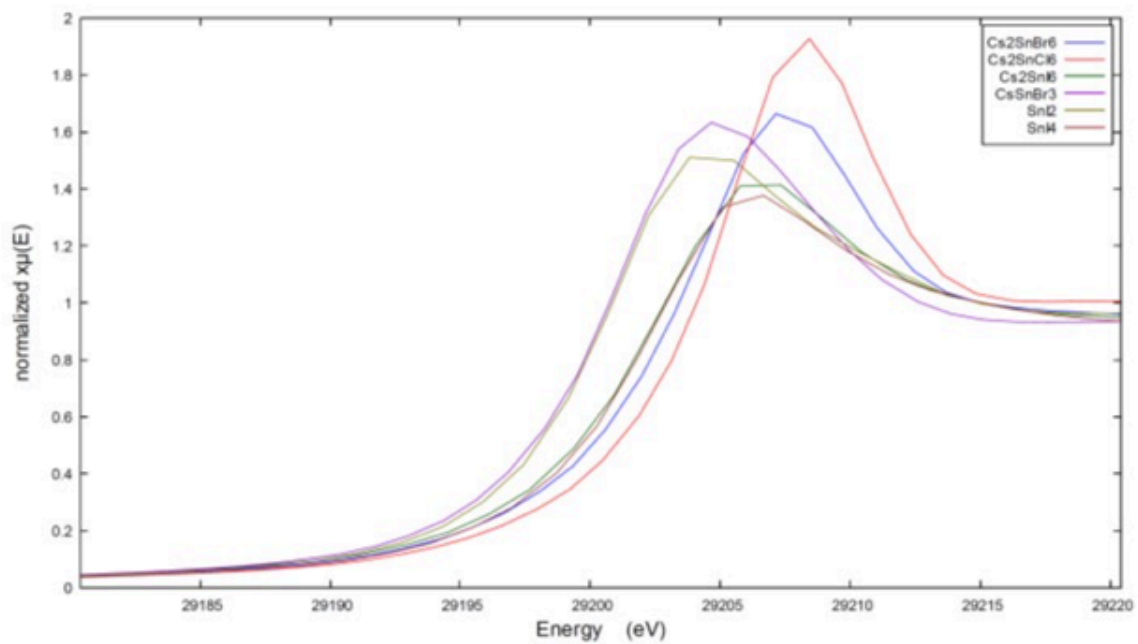


**Fig. 2:** Room temperature Sn K-edge XANES spectra of CsSnBr<sub>3</sub>, Cs<sub>2</sub>SnX<sub>6</sub> (X = Cl, Br, I), SnI<sub>2</sub> and SnI<sub>4</sub>.

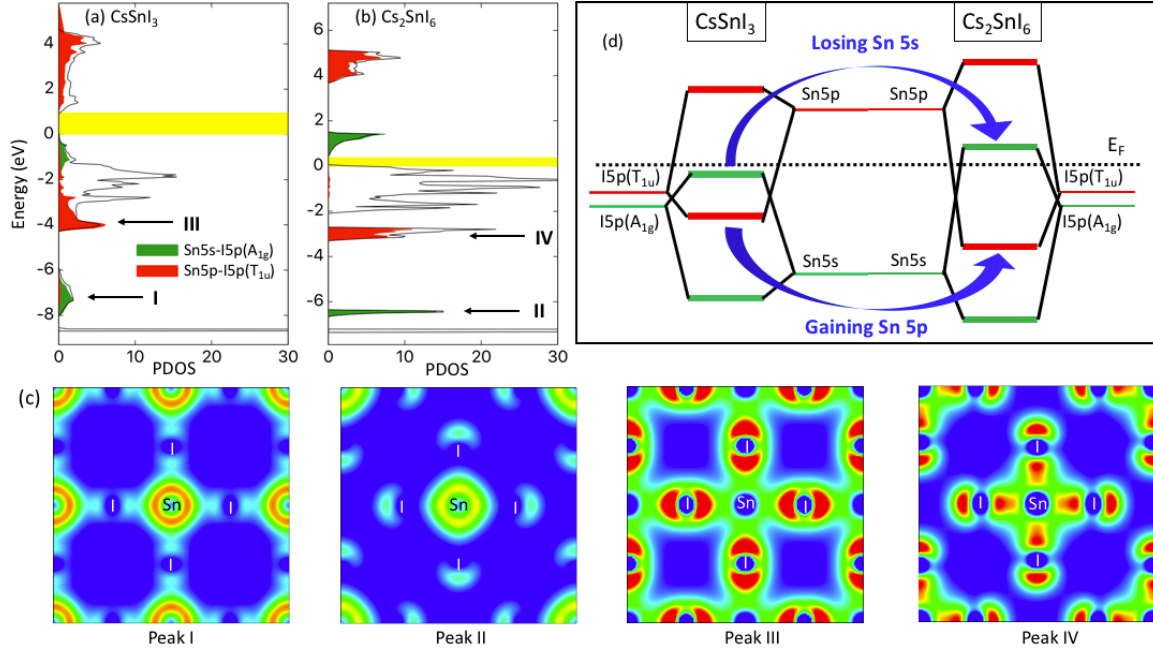


**Fig. 3:** Total density of states (DOS, black line) and its projection on the hybridization states between Sn5s and I5p A<sub>1g</sub> orbitals, and between Sn5p and I5p T<sub>1u</sub> orbitals for (a) CsSnI<sub>3</sub> and (b) Cs<sub>2</sub>SnI<sub>6</sub>. The yellow shadows indicate the band gap. (c) Partial charge density of the DOS peaks shown in (a) and (b). The [100] plane that contains both Sn and I atoms is chosen. Red areas indicate larger charge densities, whereas blue areas indicate smaller charge density. (d) Schematic diagram of Sn5s-I5p and Sn5p-I5p hybridization and the SSR mechanism for CsSnI<sub>3</sub> and Cs<sub>2</sub>SnI<sub>6</sub>.

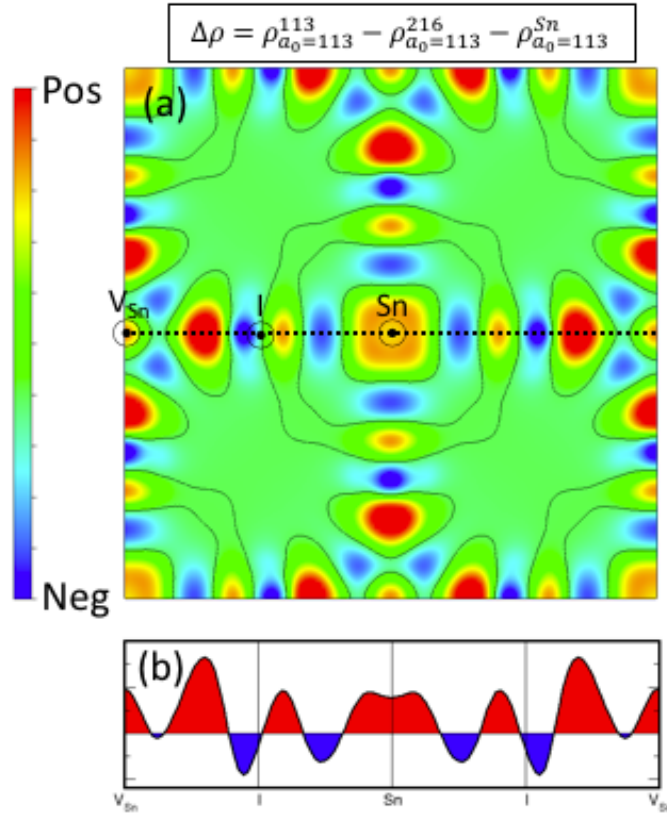


**Fig. 4:** (a) Charge density difference map calculated as  $\Delta\rho = \rho^{113} - \rho^{216} - \rho^{Sn}$ . The lattice parameter of the 113 compound was used as reference. The charge difference is displayed on the [001] plane containing Sn atoms, Sn vacancies and I atoms. (b) Profile of the charge density difference along the solid line marked in (a) shows the oscillation between charge accumulation and depletion as the function of distance away from the Sn atom. Red and blue areas denote positive and negative charge density difference, respectively.

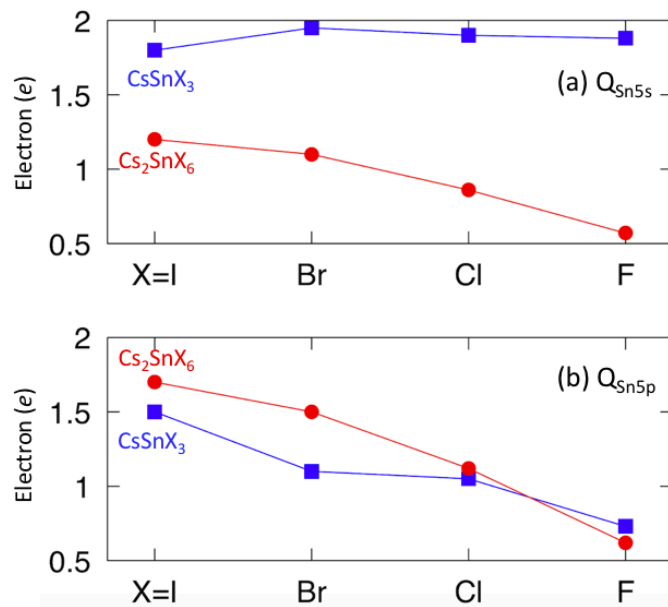


**Fig. 5:** The comparison of (a) 5s and (b) 5p component of Sn valence charge for  $\text{CsSnX}_3$  and  $\text{Cs}_2\text{SnX}_6$  ( $X = \text{I, Br, Cl}$  and  $\text{F}$ ).

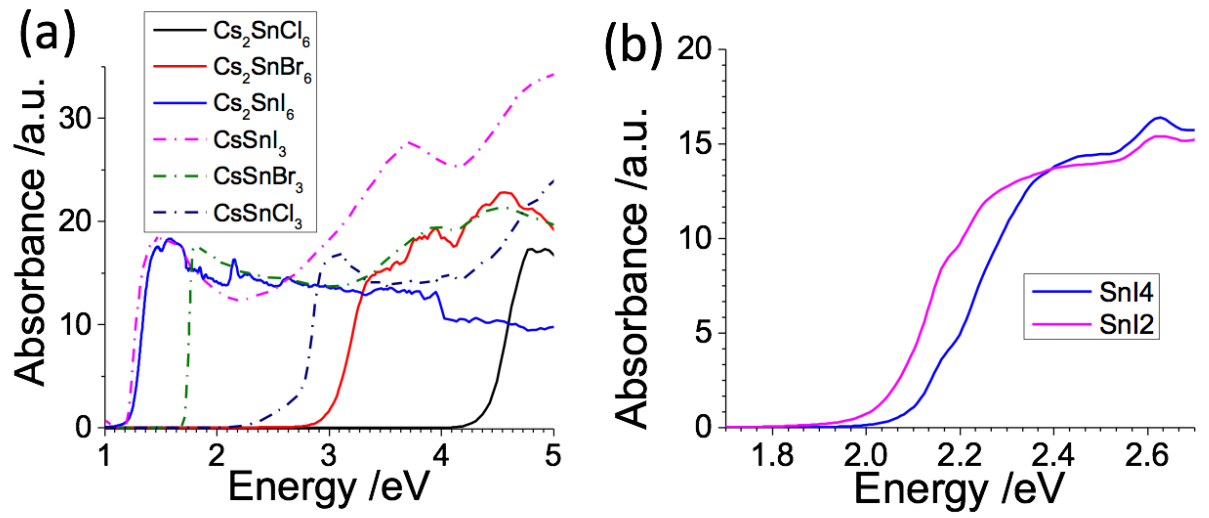


**Fig. 6.** Optical absorption spectra of (a)  $\text{CsSnBr}_3$  and  $\text{Cs}_2\text{SnX}_6$  ( $X = \text{Cl}, \text{Br}, \text{I}$ ) and (b)  $\text{SnI}_2$  and  $\text{SnI}_4$ .

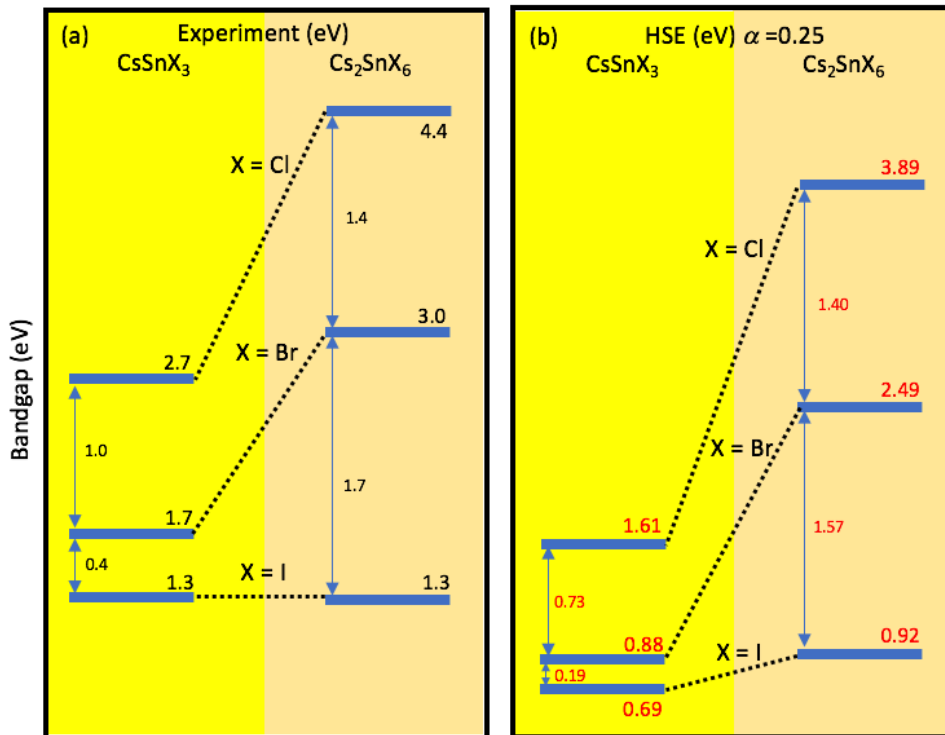


**Fig. 7:** (a) measured bandgaps for 113 and 216 halides. (b) calculated bandgaps using density functional theory and hybrid exchange-correlation functional ( $\alpha = 0.25$ ). Experimental lattice parameters were used in the calculations.

\*Authors have equally contributed to the manuscript.

- 
- [1] J. S. Manser, J. A. Christians, and P. V. Kamat, Intriguing Optoelectronic Properties of Metal Halide Perovskites, *Chem. Rev.* **116**, 12956 (2016).
- [2] B. Lee, C. C. Stoumpos, N. Zhou, F. Hao, C. Malliakas, C.-Y. Yeh, T. J. Marks, M. G. Kanatzidis, and R. P. H. Chang, Air-Stable Molecular Semiconducting Iodosalts for Solar Cell Applications: Cs<sub>2</sub>SnI<sub>6</sub> as a Hole Conductor, *J. Am. Chem. Soc.* **136**, 15379 (2014).
- [3] Bayrammurad Saparov, Jon-Paul Sun, Weiwei Meng, Zewen Xiao, Hsin-Sheng Duan, Oki Gunawan, Donghyeop Shin, Ian G Hill, Yanfa Yan, David B Mitzi, Thin-Film Deposition and Characterization of a Sn-Deficient Perovskite Derivative Cs<sub>2</sub>SnI<sub>6</sub>, *Chem. Mat.* **28**, 2315 (2016).
- [4] H. Raebiger, S. Lany, and A. Zunger, Charge self-regulation upon changing the oxidation state of transition metals and insulators, *Nature* **453**, 763 (2008).
- [5] Z. Xiao, H. Lei, X. Zhang, Y. Zhou, H. Hosono, and T. Kamiya, Ligand-Hole in [SnI<sub>6</sub>] Unit and Origin of Band Gap in Photovoltaic Perovskite Variant Cs<sub>2</sub>SnI<sub>6</sub>, *Bull. Chem. Soc. of Jap.* **88**, 1250 (2015).
- [6] G. Kresse, and J. Furthmüller, *J. Comput. Mater. Sci.* **6**, 15 (1996).
- [7] A. V. Krukau, O. A. Vydrov, A. F. Izmaylov, G. E. J. Scuseria, *Chem. Phys.* **125**, 224106 (2006).
- [8] R. Resta, Physical chemistry: Charge states in transition, *Nature* **453**, 735 (2008).
- [9] R. Resta, Macroscopic polarization in crystalline dielectrics: the geometric phase approach, *Rev. of Mod. Phys.* **66**, 899 (1994).
- [10] <https://goldbook.iupac.org/html/O/O04365.html>
- [11] L. Pauling, The modern theory of valency, *J. Chem. Soc. (Resumed)* 1461, (1948).
- [12] R. Hoffmann, *Am. Sci.* **89**, 311 (2001).
- [13] S. Johnston, A. Mukherjee, I. Elfimov, M. Berciu, and G. A. Sawatzky, Charge Disproportionation without Charge Transfer in the Rare-Earth-Element Nickelates as a Possible Mechanism for the Metal-Insulator Transition, *Phys. Rev. Lett.* **112**, 10 (2014).
- [14] M. Caldas, A. Fazio, and A. Zunger, Chemical Trends and Universalities in the Spectra of Transition Metal Impurities in Semiconductors, *J. Electron. Mat.* **14a**, 1035 (1985).
- [15] C. Wolverton and A. Zunger, First-Principles Prediction of Vacancy Order-Disorder and Intercalation Battery Voltages in Li<sub>x</sub>CoO<sub>2</sub> *Physical Review Letters* **81**, 606 (1998).
- [16] D. Tudela, A. J. Sánchez-Herencia, M. Díaz, R. Fernández-Ruiz, N. Menéndez, and J. D. Tornero, Mössbauer spectra of tin(IV) iodide complexes, *Journal of the Chemical Society, Dal. Transact.* **22**, 4019 (1999).
- [17] C. Bontschev, D. Christov, and B. Manushev, Untersuchungen von nach verschiedenen Verfahren hergestellten Zinnjodiden mit Hilfe des Mossbauer-Effektes,," *Zeitschrift fur anorganische und allgemeine Chemie* **379**, 95 (1970).
- [18] J. D. Donaldson, D. C. Puxley, and M. J. Tricker, The interpretation of the 119mSn Mössbauer data for some complexes of tin(II), *J. of Inorg. Nucl. Chem.* **37**, 655 (1975).
- [19] K. Yamada, Y. Kuranaga, K. Ueda, S. Goto, T. Okuda, and Y. Furukawa, Phase Transition and Electric Conductivity of ASnCl<sub>3</sub> (A = Cs and CH<sub>3</sub>NH<sub>3</sub>), *Bull. Chem. Soc. Jap.* **71** 127 (1998).
- [20] I. Chung, J.-H. Song, J. Im, J. Androulakis, C. D. Malliakas, H. Li, A. J. Freeman, J. T. Kenney, and M. G. Kanatzidis, CsSnI<sub>3</sub>: Semiconductor or Metal? High Electrical Conductivity and Strong Near-Infrared Photoluminescence from a Single Material. High Hole Mobility and Phase-Transitions, *J. Am. Chem. Soc.* **134**, 8579 (2012).

- 
- [21] J. D. Donaldson and J. Silver, The Mössbauer effect in tin(II) compounds. Part XIII. Data for the products from molten caesium–tin(II)–halide systems, *J. Chem. Soc., Dalton Trans.* **6**, 666 (1973).
- [22] J. W. Zwanziger, Computation of Mössbauer isomer shifts from first principles, *J. Phys.: Cond. Mat.* **21**, 195501 (2009).
- 23 P. M. A. Sherwood, Valence-band spectra of tin oxides interpreted by X $\alpha$  calculations, *Phys. Rev. B* **41**, 10151 (1990).
- [24] G. Alonzo, N. Bertazzi, J. R. Ferraro, A. Furlani, G. Iucci, G. Polzonetti, and M. V. Russo, Mössbauer, Far-Infrared, and XPS Investigations of SnCl<sub>2</sub> and SnCl<sub>4</sub> Introduced in Polyconjugated Monosubstituted Acetylene Matrices, *Appl. Spectr.* **49**, 237 (1995).
- [25] K. P. Marshall, R. I. Walton, and R. A. Hatton, Tin perovskite/fullerene planar layer photovoltaics: improving the efficiency and stability of lead-free devices, *J. Mater. Chem. A* **3**, 11631 (2015).
- [26] S. Kraft, J. Stümpel, P. Becker, and U. Kuetsgens, High resolution x-ray absorption spectroscopy with absolute energy calibration for the determination of absorption edge energies, *Rev. Sci. Instr.* **67**, 681 (1996).
- [27] C. A. Clausen and M. L. Good, Interpretation of the Moessbauer spectra of mixed-hexahalo complexes of tin(IV), *Inorg. Chem.* **9**, 817 (1970).
- [28] R. H. Herber, Structure, Bonding, and the Mossbauer Lattice Temperature, *Chem. Mössb. Spectr.* 199 (1984).

## Supplementary Materials

### Changes in charge density vs changes in formal oxidation states: The case of Sn halide perovskites and their ordered vacancy analogues

Gustavo M. Dalpian,<sup>1,2,\*</sup> Qihang Liu,<sup>1,\*</sup> Constantinos C. Stoumpos,<sup>3,\*</sup> Alexios P. Douvalis,<sup>4</sup>  
Mahalingam Balasubramanian,<sup>5</sup> Mercouri G. Kanatzidis,<sup>3,6</sup> Alex Zunger<sup>1</sup>

<sup>1</sup>*Renewable and Sustainable Energy Institute, University of Colorado, Boulder, Colorado 80309, USA*

<sup>2</sup>*Centro de Ciências Naturais e Humanas, Universidade Federal do ABC, Santo André, SP, Brazil*

<sup>3</sup>*Materials Science Division, Argonne National Laboratory, Argonne, Illinois 60439, USA*

<sup>4</sup>*Physics Department, University of Ioannina, 45110 Ioannina, Greece*

<sup>5</sup>*Advanced Photon Source, Argonne National Laboratory, Argonne, IL 60439, United States*

<sup>6</sup>*Department of Chemistry, Northwestern University, Evanston, Illinois 60208, USA*

## S1 Synthesis

**a) Preparation of the  $Cs_2SnX_6$  compounds.**  $Cs_2SnX_6$  compounds were prepared following a modification of a reported method.<sup>1</sup> In a typical procedure,  $SnO_2$  (3.01g, 20mmol) was dissolved in an excess (20 mL) of the corresponding concentrated, aqueous hydrohalic acid (HCl: 35% w/w; HBr: 48% w/w; HI: 57% w/w) under heating to 110°C. A CsX solution was prepared separately by dissolving  $Cs_2CO_3$  (6.52g, 20mmol) in 10 mL of the corresponding acid. Mixing the two solutions under vigorous stirring resulted in the immediate precipitation of a fine powder ( $Cs_2SnCl_6$ : white;  $Cs_2SnBr_6$ : tan;  $Cs_2SnI_6$ : black). The reaction was continued for a further 10 min following the addition of deionized  $H_2O$  (5 mL) to facilitate the stirring of the dense mixture and ensure completion of the reaction. The solid was subsequently filtered under vacuum and washed copiously with absolute EtOH followed by drying at 60°C under vacuum. Yield >95% (manipulative losses).

**b) Preparation of the  $CsSnBr_3$ .**  $CsSnBr_3$  was prepared following a modification of a reported method.<sup>2</sup> In a typical procedure, stoichiometric ratios of  $SnBr_2$  (20 mmol, 5.570 g) and CsBr (20 mmol, 4.256 g) were placed in a fused  $SiO_2$  tube, evacuated at  $10^{-3}$  mbar and flame-sealed. The silica tube was placed in a furnace and heated to 600 °C over over 6 h, held at this temperature for 3 h, followed by cooling down to ambient temperature over 3 h, yielding quantitatively a shiny black ingot.

**c) Preparation of the  $SnI_2$  and  $SnI_4$  compounds.**  $SnI_2$  was prepared following a modification of a reported method.<sup>3</sup> In a typical procedure, an excess of granulated Sn (50g) and  $I_2$  (70g) were combined in 400 mL of a 2M aqueous HCl under a  $N_2$  blanket. Upon completion of the reaction, the hot yellow solution was slowly brought to ambient temperature where  $SnI_2$  crystallizes as long red needles after standing for 1 day. Yield ~60-70% (based on  $I_2$ ). Crude  $SnI_2$  can be isolated quantitatively by evaporation of the supernatant liquid to dryness.  $SnI_4$  was prepared by combination of Sn (5.94g, 50 mmol) and  $I_2$  (25.38g, 100mmol) in boiling toluene (100 mL) under reflux. The reaction mixture is heated to boiling under reflux conditions. After completion of the reaction the solution is cooled to ambient temperature to precipitate orange octahedral crystals of  $SnI_4$ . The crystals are filtered and dried thoroughly under vacuum. Yield ~70%. Crude  $SnI_4$  can be isolated quantitatively by evaporation of the supernatant liquid to dryness.

## S2 Experimental Characterization

### a) Determination of the crystal structure parameters.

Powder X-ray diffraction (PXRD) data for  $\text{Cs}_2\text{SnX}_6$  were collected in the  $2\theta = 5\text{-}140^\circ$  on a Rigaku Miniflex 600 equipped with a Cu  $K\alpha$  source ( $\lambda = 1.5406 \text{ \AA}$ ) operating at 40kV and 15 mA. High-resolution temperature dependent powder X-ray diffraction data for  $\text{CsSnBr}_3$  and  $\text{CsSnI}_3$  were collected at Advance Photon Source (11-BM). The data were refined using JANA2006<sup>4</sup>. Fig S1 shows the crystal structures of all samples and figs S2-S5 show the PXRD patterns.

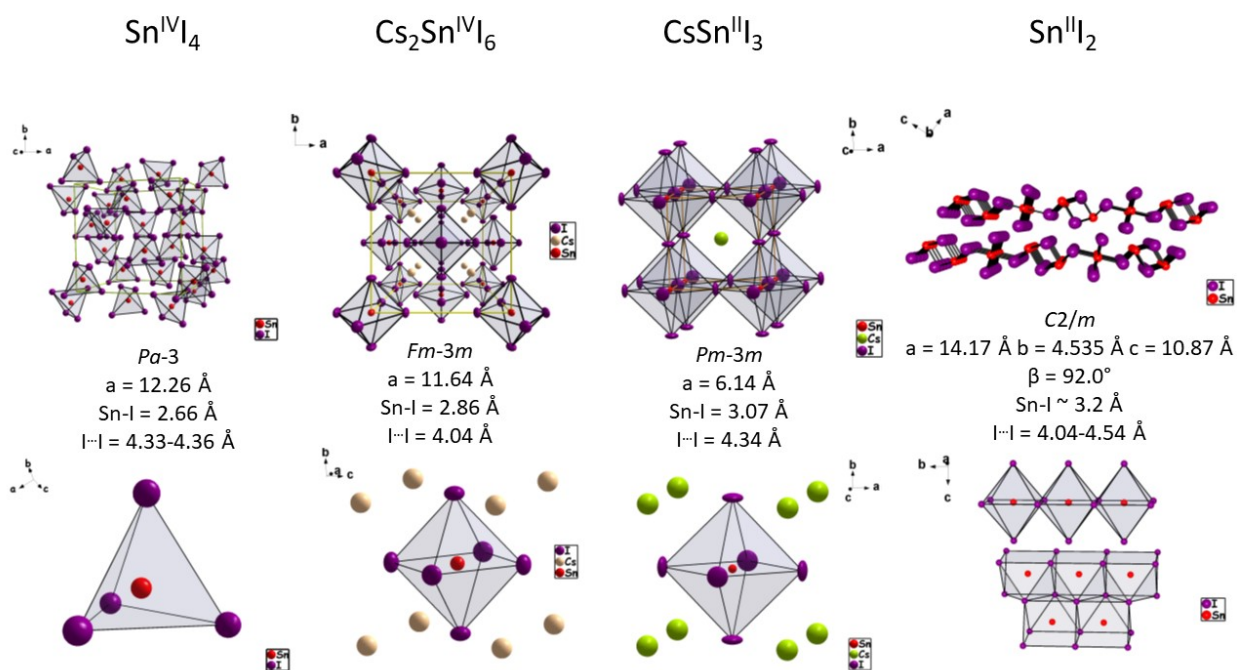


**Figure S1.** Crystal structures of (top)  $\text{SnI}_4$ ,  $\text{Cs}_2\text{SnI}_6$ ,  $\text{CsSnI}_3$  and  $\text{SnI}_2$  and (bottom) the corresponding building blocks of the inorganic lattices.

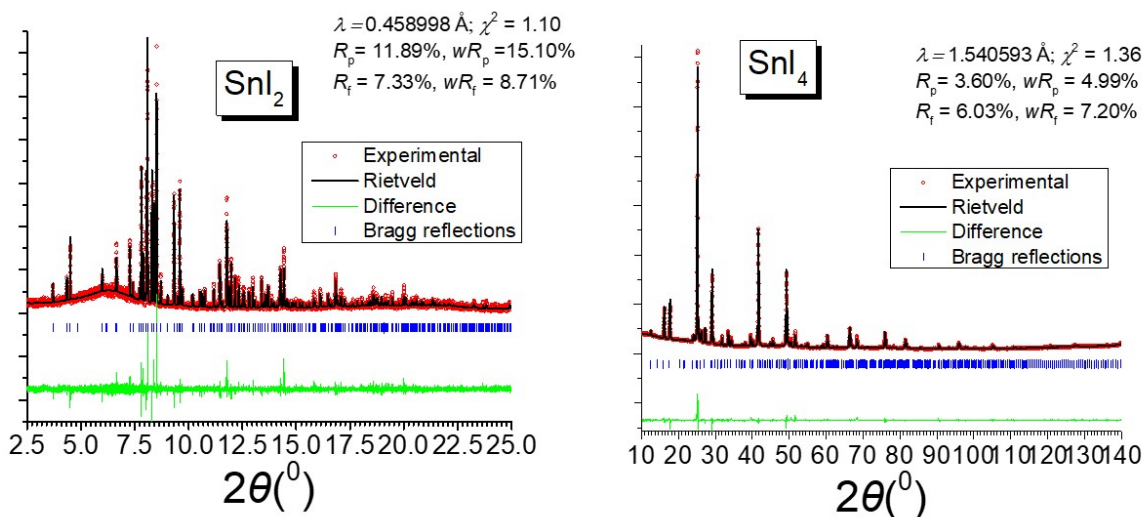


Figure S2. PXRD patterns of SnI<sub>2</sub> and SnI<sub>4</sub> at room temperature.

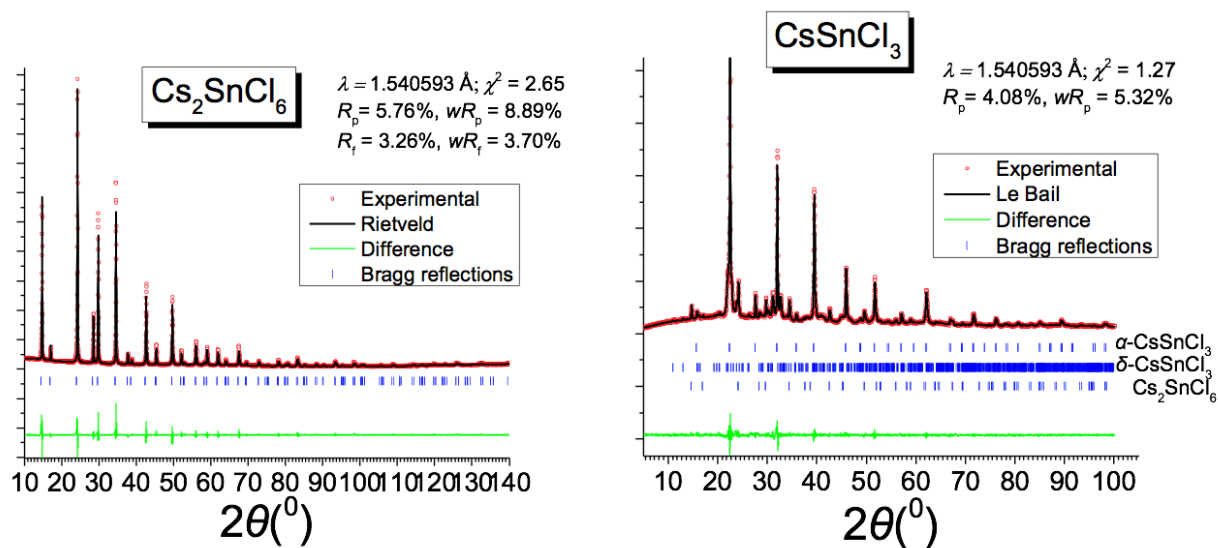
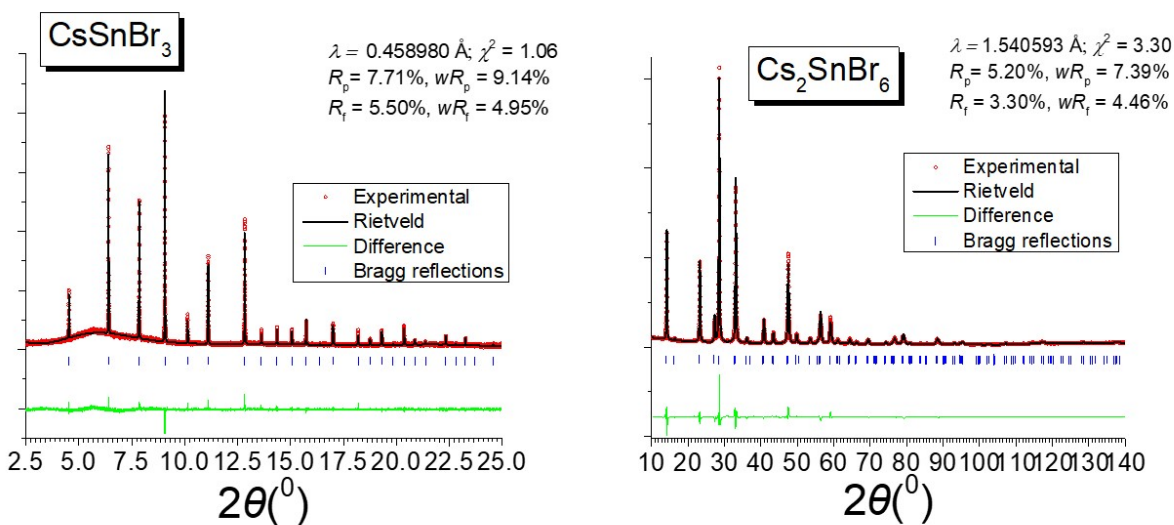
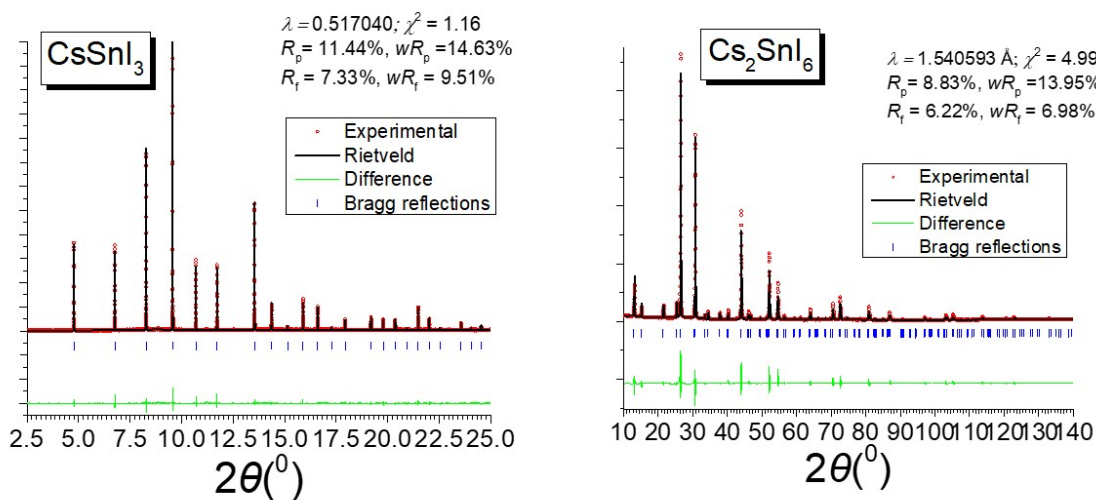


Figure S3. PXRD patterns of Cs<sub>2</sub>SnCl<sub>6</sub> and CsSnCl<sub>3</sub> at room temperature. The latter is metastable and transitions from the metastable  $\alpha\text{-CsSnCl}_3$  phase (cubic perovskite) to the stable  $\delta\text{-CsSnCl}_3$  phase (monoclinic phase). Partial oxidation to Cs<sub>2</sub>SnCl<sub>6</sub> also occurs gradually.



**Figure S4.** PXRD patterns of CsSnI<sub>3</sub> (500K) and Cs<sub>2</sub>SnI<sub>6</sub> (293K).



**Figure S5.** PXRD patterns of CsSnBr<sub>3</sub> and Cs<sub>2</sub>SnBr<sub>6</sub> at room temperature.

**b) K-Edge Sn XAS spectroscopy.** K-edge X-ray absorption spectra were collected on pressed pellets (6mm diameter, 2mm thickness) of CsSnX<sub>3</sub>, Cs<sub>2</sub>SnX<sub>6</sub>, SnI<sub>2</sub> and SnI<sub>4</sub>. The samples were prepared by mixing 17 mg of the Sn compounds with 85 mg of dry BN following by homogenization of the powders using mortar and pestle. The homogeneous mixtures were pressed in a hydraulic press using a pressure of ~0.35 GPa to form dense pellets. The pellets were measured at Advanced Photon Source (Beamline 20-ID) in the 29050-30427 keV range using a step of 5 eV for the pre-edge region, 1.5 eV for the edge region and 0.05eV for the post-

edge region with an integration time of 1s. The spectra were measured against a Sn foil standard. The data were processed and analyzed using Demeter.<sup>5</sup>

c) ***<sup>119</sup>Sn Mössbauer Spectroscopy.*** <sup>119</sup>Sn Mössbauer spectra were collected on powder samples using a constant-acceleration Mössbauer spectrometer equipped with a Ca<sup>119m</sup>SnO<sub>3</sub> source kept at room temperature (RT = 291-293 K) and a variable-temperature cryostat (Thor Cryogenics). The spectrometer was calibrated with metallic  $\alpha$ -Fe at RT. Analyses of the spectra were performed using a least-squares Mössbauer fitting program [Douvalis, A. P.; Polymeros, A.; Bakas, T. J. Phys.: Conf. Ser. 2010, 217, 012014.] and the isomer shift (IS) values of the components used to fit the spectra are given relative to SnO<sub>2</sub> at RT.

**Table S1.** Selected <sup>119</sup>Sn Mössbauer parameters for CsSnX<sub>3</sub>, Cs<sub>2</sub>SnX<sub>6</sub>, SnI<sub>2</sub> and SnI<sub>4</sub>

Sample	Isomer Shift (mm/s)	$\Gamma/2$ (mm/s)	Quadrupole splitting (mm/s)	Area (%)	FOS
SnI <sub>4</sub>	<b>1.48</b>	0.11	0.00	100	Sn <sup>IV</sup> in $\alpha$ -SnI <sub>4</sub>
SnI <sub>2</sub>	-0.01	0.36	0.53	83	Sn <sup>IV</sup> in $\alpha$ -SnO <sub>2</sub>
	<b>3.87</b>	0.31	0.17	17	Sn <sup>II</sup> in $\alpha$ -SnI <sub>2</sub>
Cs <sub>2</sub> SnI <sub>6</sub>	<b>1.32</b>	0.39	0.00	100	Sn <sup>IV</sup> in $\alpha$ -Cs <sub>2</sub> SnI <sub>6</sub>
Cs <sub>2</sub> SnCl <sub>6</sub>	<b>0.46</b>	0.39	0.12	100	Sn <sup>IV</sup> in $\alpha$ -Cs <sub>2</sub> SnCl <sub>6</sub>
Cs <sub>2</sub> SnBr <sub>6</sub>	<b>0.83</b>	0.37	0.17	100	Sn <sup>IV</sup> in $\alpha$ -Cs <sub>2</sub> SnBr <sub>6</sub>
CsSnBr <sub>3</sub>	0.044	0.33	0.51	5	Sn <sup>IV</sup> in $\alpha$ -SnO <sub>2</sub>
	<b>3.90</b>	0.37	0.15	95	Sn <sup>II</sup> $\alpha$ -CsSnBr <sub>3</sub>

### S3 Theoretical Calculations

The *ab initio* calculations were performed by using plane-wave pseudopotential approach within density functional theory (DFT) as implemented in the Viena Ab Initio Simulation Package (VASP).<sup>6, 7</sup> We've used the projected augmented wave pseudopotentials<sup>7</sup> with a valence configuration as: Cs(5s<sup>2</sup>5p<sup>6</sup>6s<sup>1</sup>), Sn(5s<sup>2</sup>2p<sup>2</sup>), F(2s<sup>2</sup>2p<sup>5</sup>), Cl(3s<sup>2</sup>3p<sup>5</sup>), Br(4s<sup>2</sup>4p<sup>5</sup>) and I(5s<sup>2</sup>5p<sup>5</sup>). The generalized gradient approximation formulated by Perdew, Burke, and Ernzerhof (PBE)<sup>8</sup> is used as exchange correlation functional. Experimental lattice parameters and atomic positions were used through the calculations. These are very good models since we are mostly interested on the change density differences. K-point sets of 10x10x10 for 113 compounds and 6x6x6 for 216 compounds were used. To reduce the self-interaction error of DFT for band gaps and band structured calculations, we used the Heyd-Scuseria-Ernzerhof (HSE) hybrid functional approach with standard 25% exact Fock exchange included.<sup>9</sup>

## S4 Structural properties for 113 and 216 compounds

In order to form the 216 compound, Sn atoms are removed from 113 in such a way that a stacking between planes of vacancies and of Sn atoms are formed in the (111) direction, as shown in Figure S1. The removal of 50% of the atoms leads to strong relaxations, significantly decreasing the bond length between Sn and I atoms and thus the volume of the [SnI6] octahedron. Table SI shows measured lattice parameters for the halide compounds. We note that there is a -8% difference in the Sn-I bond length for the Cs<sub>2</sub>SnI<sub>6</sub> compared with CsSnI<sub>3</sub>. On the other hand, the Shannon-Prewitt effective ionic radius for Sn is 0.69 Å for Sn (IV+) and 0.96 Å for Sn(II+), with a much larger difference (-28%). This raises interesting questions on how the physical charges relate to the FOS of the Sn atoms in these perovskite compounds.

**Table S2:** experimental structural parameters for halides.

A <sub>n</sub> MX <sub>3n</sub>	Cs <sub>2</sub> SnI <sub>6</sub>	CsSnI <sub>3</sub> (500K)	Cs <sub>2</sub> SnBr <sub>6</sub>	CsSnBr <sub>3</sub>	Cs <sub>2</sub> SnCl <sub>6</sub>	CsSnCl <sub>3</sub> <sup>10</sup>
Structure	cubic	Cubic	cubic	cubic	cubic	cubic
space group	<i>Fm-3m</i>	<i>Pm-3m</i>	<i>Fm-3m</i>	<i>Pm-3m</i>	<i>Fm-3m</i>	<i>Pm-3m</i>
a (Å)	11.6276(9)	6.20589(1)	10.8265(2)	5.7956(7)	10.3721(2)	5.504
d(x-x) (Å)	4.0332(6)	4.38819(3)	3.713(1)	4.0981(5)	3.483(3)	3.892
d(m-x) (Å)	2.8519(6)	3.10295(2)	2.625(1)	2.8978(4)	2.463(3)	2.752
d(a-x) (Å)	4.1113(3)	4.38819(3)	3.8286(1)	4.0981(5)	3.6694(1)	3.892

## S5 Band structures for 113 and 216 compounds calculated with hybrid functionals

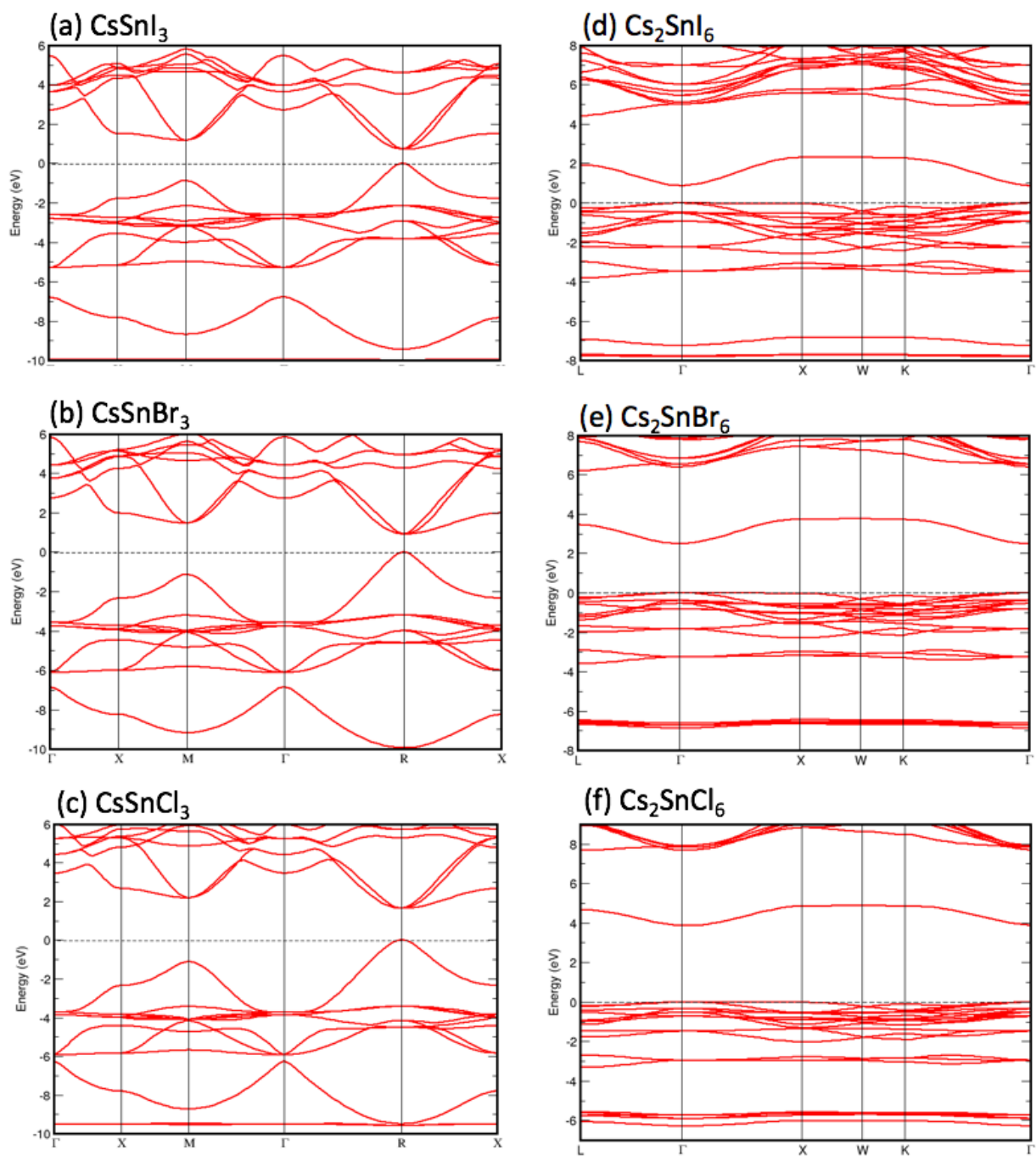


**Figure S6.** Band structures of halide perovskites. Dotted lines indicate the valence band maximum. All calculations were performed using hybrid functionals and the experimental lattice parameters.

S6 Charge density difference at the 216 lattice parameter.

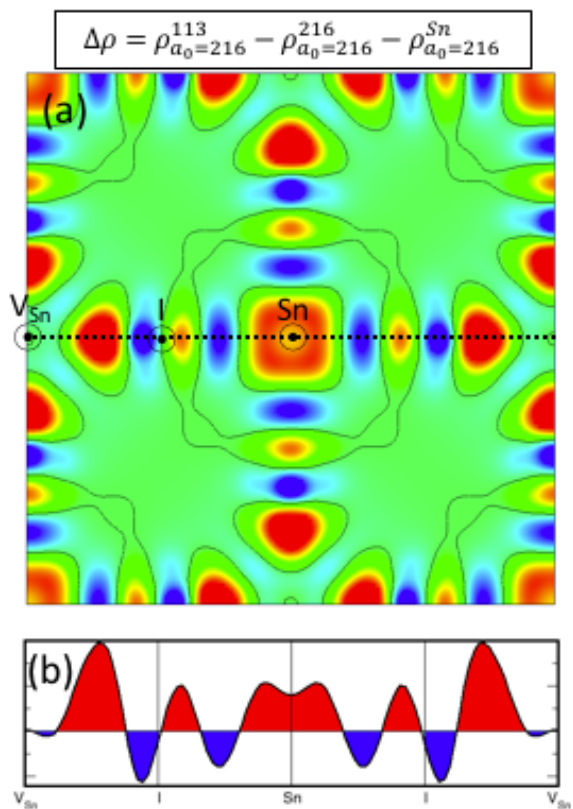
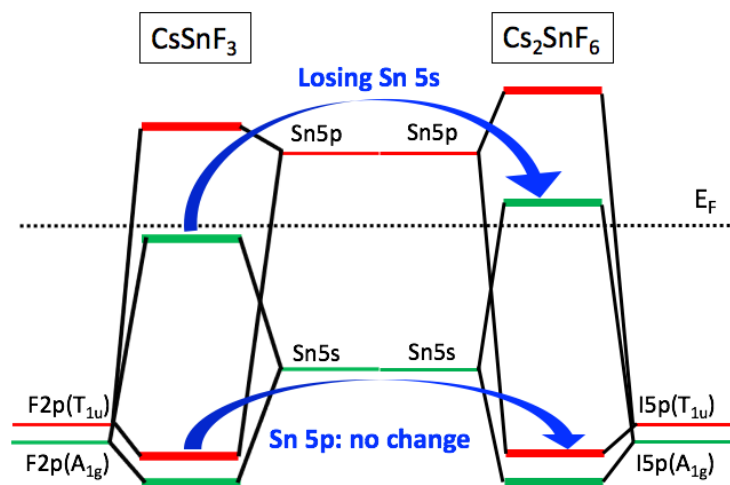


Fig. S6: Charge density difference at the 216 compound lattice parameter.

## S7 Band diagram for the fluorides



**Fig. S7:** Energy diagram for fluorides showing the inversion of the energetic order of F2p and Sn5s levels, minimizing the SRR effect.

### S8. The fully ionic limit: CsSrI<sub>3</sub>

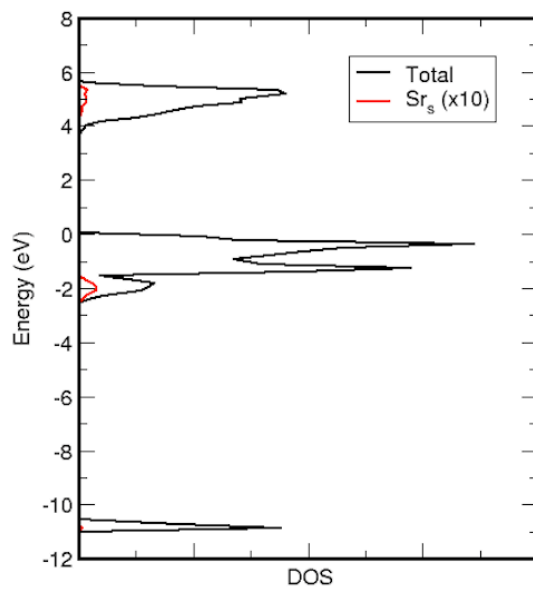


**Figure S8.** Projected density of states for CsSrI<sub>3</sub>. The Sr s contribution is very small, indicating the fully ionic, FOS IV limit.

### S9. The relevance of the SnX6 molecule to the discussion above

The progression from 113 to 216 and then to the isolated  $[\text{SnI}_6]^{2-}$  molecule reveals the trend of the bands becoming narrower and more localized as the  $\text{SnI}_6$  units are more separated: By comparing the total DOS of the two iodides, we find that  $\text{CsSnI}_3$  has broader DOS bands, while  $\text{Cs}_2\text{SnI}_6$  has sharper DOS peaks (see Fig 2a and b). This is because the main contribution to states near the Fermi level is from the  $\text{SnI}_6$  octahedron, which has higher packing density in the 113 compounds (with corner sharing octahedra) whereas in the 216 compounds the octahedra are discrete and isolated. We also considered the electronic structure of the hypothetical molecular limit of a  $[\text{SnI}_6]^{2-}$  octahedron as comparison. The results (Fig. S8) illustrate that the dominant hybridization in 216 is inside each  $[\text{SnI}_6]^{2-}$  octahedron.

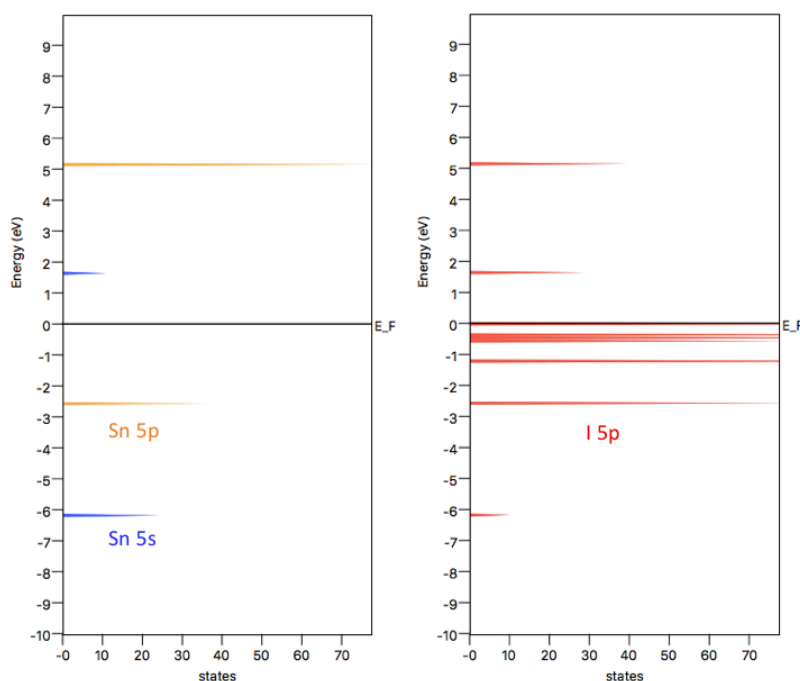


Fig. S9: projected DOS of  $[\text{SnI}_6]^{2-}$  molecule.

## References:

- [1] B. Lee, C. C. Stoumpos, N. Zhou, F. Hao, C. Malliakas, C.-Y. Yeh, T. J. Marks, M. G. Kanatzidis, and R. P. H. Chang, Air-Stable Molecular Semiconducting Iodosalts for Solar Cell Applications: Cs<sub>2</sub>SnI<sub>6</sub> as a Hole Conductor, *J. Am. Chem. Soc.* **136**, 15379 (2014).
- [2] D. H. Fabini, G. Laurita, J. S. Bechtel, C. C. Stoumpos, H. A. Evans, A. G. Kontos, Y. S. Raptis, P. Falaras, A. Van der Ven, M. G. Kanatzidis, and R. Seshadri, Dynamic Stereochemical Activity of the Sn<sup>2+</sup>+Lone Pair in Perovskite CsSnBr<sub>3</sub>, *J. Am. Chem. Soc.* **138**, 11820 (2016).
- [3] C. C. Stoumpos, C. D. Malliakas, and M. G. Kanatzidis, Semiconducting Tin and Lead Iodide Perovskites with Organic Cations: Phase Transitions, High Mobilities, and Near-Infrared Photoluminescent Properties, *Inorg. Chem.* **52**, 9019 (2013).
- [4] V. Petříček, M. Dušek, and L. Palatinus, Crystallographic Computing System JANA2006: General features, *Zeitschrift für Kristallographie - Crystalline Materials* **229**, 5 (2014).
- [5] B. Ravel and M. Newville, ATHENA, ARTEMIS, HEPHAESTUS: data analysis for X-ray absorption spectroscopy using IFEFFIT, *J. of Synch. Rad.* **12**, 537 (2005).
- 6 G. Kresse, and J. Furthmüller, *J. Comput. Mater. Sci.* **6**, 15 (1996).
- 7 G. Kresse, and D. Joubert, *Phys. Rev. B* **59**, 1758 (1999).
- 8 J. P. Perdew, K. Burke, and M. Ernzerhof, *Phys. Rev. Lett.* **77**, 3865 (1996).
- 9 A. V. Krukau, O. A. Vydrov, A. F. Izmaylov, G. E. J. Scuseria, *Chem. Phys.* **125**, 224106 (2006).
- [10] G. G. Bulanova, A. B. Podlesskaya, L. V. Soboleva, A. I. Soklakov, Study of Caesium tin chloride CsSnCl<sub>3</sub> and Cs<sub>2</sub>SnCl<sub>6</sub> *Izvestiya Akademii Nauk SSSR, Neorganicheskie Materialy* **8**, 1930 (1972).